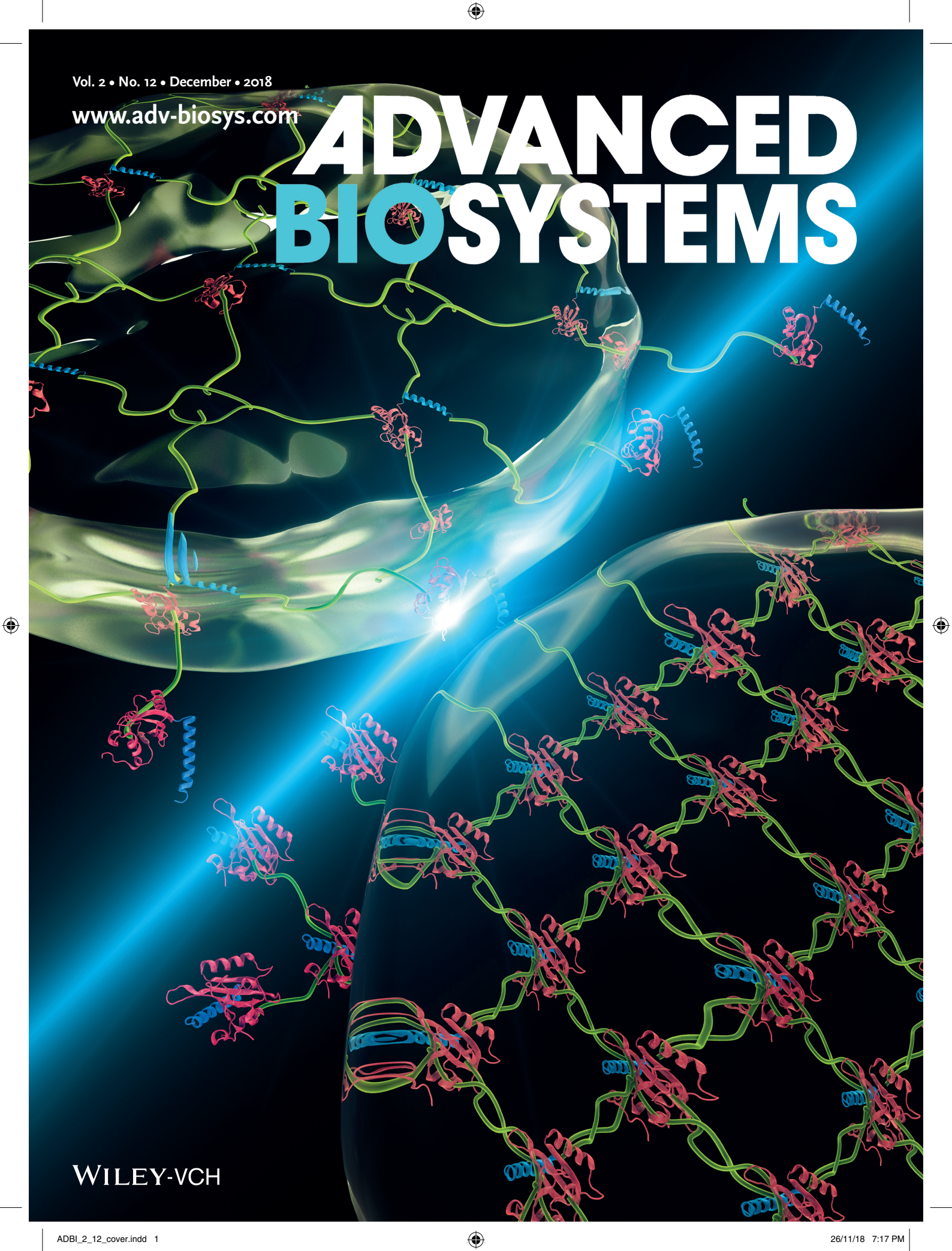


Vol. 2 • No. 12 • December • 2018

[www.adv-biosys.com](http://www.adv-biosys.com)

# ADVANCED BIOSYSTEMS



WILEY-VCH

# Cyclic Stiffness Modulation of Cell-Laden Protein–Polymer Hydrogels in Response to User-Specified Stimuli Including Light

Luman Liu, Jared A. Shadish, Christopher K. Arakawa, Kevin Shi, Jennifer Davis, and Cole A. DeForest\*

Although mechanical signals presented by the extracellular matrix are known to regulate many essential cell functions, the specific effects of these interactions, particularly in response to dynamic and heterogeneous cues, remain largely unknown. Here, a modular semisynthetic approach is introduced to create protein–polymer hydrogel biomaterials that undergo reversible stiffening in response to user-specified inputs. Employing a novel dual-chemoenzymatic modification strategy, fusion protein-based gel crosslinkers are created that exhibit stimuli-dependent intramolecular association. Linkers based on calmodulin yield calcium-sensitive materials, while those containing the photosensitive light, oxygen, and voltage sensing domain 2 (LOV2) protein give phototunable constructs whose moduli can be cycled on demand with spatiotemporal control about living cells. These unique materials are exploited to demonstrate the significant role that cyclic mechanical loading plays on fibroblast-to-myofibroblast transdifferentiation in 3D space. The moduli-switchable materials should prove useful for studies in mechanobiology, providing new avenues to probe and direct matrix-driven changes in 4D cell physiology.

There is a growing appreciation for the large role that mechanical signals presented by the local extracellular matrix (ECM) have on cell function. Through direct interaction with physical cues presented in the cellular ECM, these external mechanical signals are translated into internal biochemical responses that govern gene expression and cell fate decisions.<sup>[1]</sup> Seminal findings in the field of cellular mechanotransduction have demonstrated that matrix stiffness alone can drive changes in essential processes including attachment, cytoskeletal organization, migration, proliferation, and differentiation.<sup>[2–4]</sup> More recently, it has been observed that cells possess mechanical “memory,” storing information about past physical culture conditions to influence future behaviors.<sup>[5]</sup> These findings represent landmark observations that are rapidly changing standard practices in molecular biology and stem cell culture.

Efforts to elucidate the specific effects that ECM stiffness and elasticity have on cell physiology have been performed almost exclusively using static biomaterials. While these studies have provided invaluable insight into the critical roles in which ECM stiffness regulates cellular fate, such simple systems fail to emulate biophysical dynamics known to accompany tissue/organ development, regeneration, and disease progression. Strategies to probe the biological effects of evolving tissue compliance have yielded a variety of synthetic cell culture platforms that can either soften or stiffen over time.<sup>[6]</sup> Though constructs that undergo spontaneous or cell-mediated transitions have proven beneficial in several applications, those that can be modified on demand are critical for probing biophysical responses at well-defined times.<sup>[7]</sup> Light-mediated material alteration has proven particularly beneficial in this regard as it uniquely grants near-instantaneous and spatiotemporal control over matrix stiffness in a potentially biocompatible manner.<sup>[8]</sup> Material secondary photo-crosslinking enables one-way stiffening,<sup>[9–14]</sup> while photodegradation provides for irreversible softening,<sup>[15–19]</sup> in the presence of live cells.

Beyond unidirectional elasticity changes, cells also experience cyclic loading that periodically and reversibly alter local ECM rigidity; pulsatile flow associated with the circulatory system

L. Liu, J. A. Shadish, Prof. C. A. DeForest  
Department of Chemical Engineering  
University of Washington  
3781 Okanogan Lane NE, Seattle, WA 98195, USA  
E-mail: ProfCole@uw.edu

C. K. Arakawa, K. Shi, Prof. J. Davis, Prof. C. A. DeForest  
Department of Bioengineering  
University of Washington  
3720 15th Ave NE, Seattle, WA 98105, USA

Prof. J. Davis  
Department of Pathology  
University of Washington  
1959 NE Pacific St., Seattle, WA 98195, USA

Prof. J. Davis, Prof. C. A. DeForest  
Institute for Stem Cell & Regenerative Medicine  
University of Washington  
850 Republican St., Seattle, WA 98109, USA

Prof. C. A. DeForest  
Molecular Engineering & Sciences Institute  
University of Washington  
3946 W Stevens Way NE, Seattle, WA 98195, USA

 The ORCID identification number(s) for the author(s) of this article can be found under <https://doi.org/10.1002/adbi.201800240>.

DOI: 10.1002/adbi.201800240

places cyclic loads on cells virtually everywhere throughout the body (timescale of seconds), just as tissues exhibit sequential stiffening and softening during wound healing (days to weeks). Despite significant interest in understanding these fundamental biological processes,<sup>[6,20–23]</sup> materials capable of recapitulating such dynamic and reversible stiffening remain largely undeveloped. Though several reversibly compliant biomaterials sensitive to a variety of stimuli have been reported,<sup>[24–36]</sup> none have proven capable of examining changes in 3D cell response to cyclic moduli alteration, for example, owing to cytotoxic conditions required for material formulation/modification or by unavoidable interference in material modulation chemistries by nonspecific interactions with cell culture media components. Moreover, though local heterogeneities guide cell fate anisotropically within tissues, spatial control over reversible stiffening in materials compatible with 3D cell culture has not been previously demonstrated.

Here, we introduce a generalizable strategy to create hydrogel biomaterials whose moduli can be reversibly switched in response to user-specified inputs, potentially with spatial control, and then use these unique materials to probe the effects of cyclic mechanical loading on encapsulated cell fate. Wedding changes of biomolecular conformation to those in gel crosslinking density, we genetically fuse stimuli-responsive proteins with their stimuli-dependent binding partners (**Figure 1a**). In the presence of the external stimulus, the responsive protein undergoes a conformational change that promotes binding to its fused partner and a shortened end-to-end length. Following removal of this stimulus (or introduction of another), intramolecular protein–protein

interactions are destroyed and original protein conformation is restored. When these fusion proteins are incorporated into the hydrogel crosslinker itself, molecular shortening translates to an elastic stiffening of the network, while the extended conformation yields a softer material (**Figure 1b**). As stimuli introduction and removal can be repeated ad infinitum, fully reversible control over biomaterial mechanical properties is readily obtained. Since several hundred proteins have been determined to undergo stimuli-dependent binding with known partners,<sup>[37]</sup> many smart moduli-switchable materials responsive to distinct classes of stimuli (e.g., ligands, pH, temperature, ions, light) can be readily produced.

To generate stiffness-cyclable hydrogels, we perform a step-growth polymerization via a strain-promoted azide–alkyne cycloaddition (SPAAC) between a four-arm poly(ethylene glycol) (PEG) tetrabicyclononyne (tetraBCN) ( $M_n \approx 20$  kDa), a linear PEG diazide ( $N_3$ –PEG– $N_3$ ,  $M_n \approx 3.5$  kDa), and a fusion protein uniquely end-functionalized with reactive azides ( $-N_3$ ) at both the N- and C-termini (Methods S1–S4, Supporting Information). Though SPAAC's bioorthogonality has been previously utilized to formulate cell-laden peptide–polymer hydrogels that exhibit idealized structure and well-defined composition,<sup>[18,38–42]</sup> this chemistry has not yet been exploited to create protein–polymer networks. Furthermore, precisely installed bioorthogonal handles enable almost any protein species to be used as a crosslinker without the loss-of-activity typical of site-directed mutagenesis or the uncontrollable heterogeneity that accompanies statistical functionalization of endogenous amino acid residues.<sup>[43]</sup> By varying the ratio of the azide-modified crosslinkers (i.e.,  $N_3$ –PEG– $N_3$  vs fusion protein) present

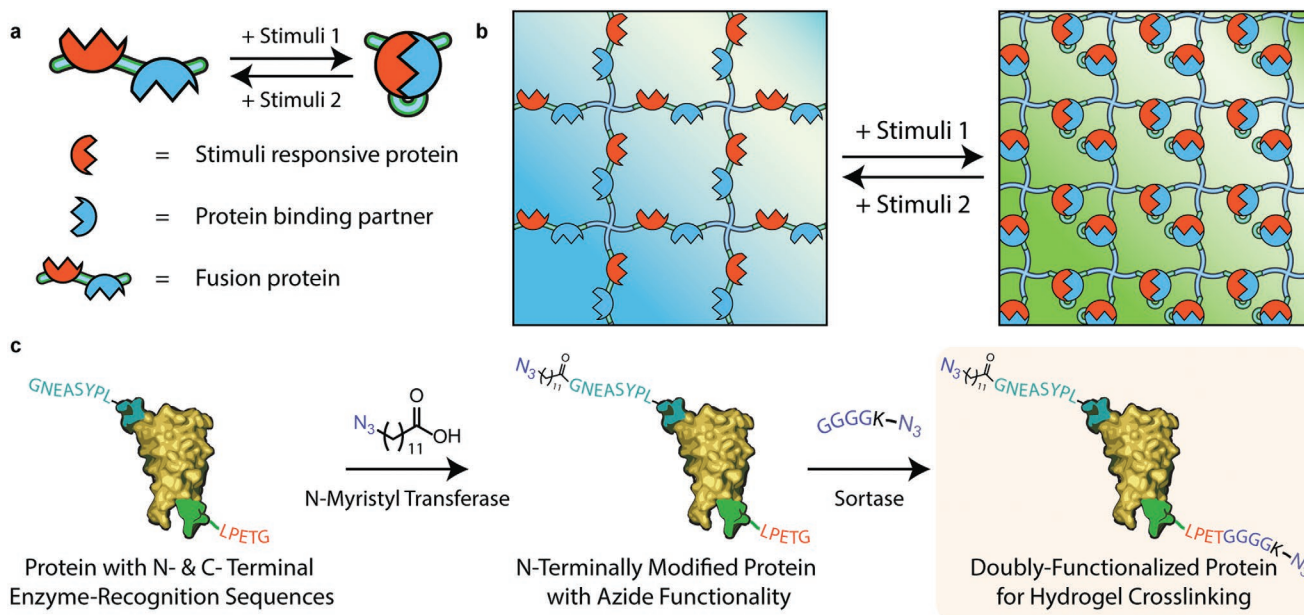


**Figure 1.** Stimuli-responsive end-functionalized protein crosslinkers. a) Genetically encoded fusion molecules between stimuli-dependent responsive proteins with their binding partners exhibit altered conformations and end-to-end lengths in response to external stimuli. b) When incorporated as a material crosslinker, intramolecular associations within the fusion protein yields reversible stimuli-dependent material stiffening. c) Recombinant fusion proteins bearing the N-terminal GNEASYPL sequence are readily myristoylated with 12-azidododecanoic acid (12-ADA) by *N*-myristoyl transferase (NMT). Species containing the C-terminal LPETG sequence can be modified via a sortase-mediated transpeptidation with an azide-functionalized polyglycine probe. These chemoenzymatic reactions can be performed sequentially on proteins that contain both the peptide motifs; the final protein is end-functionalized with reactive azides, which are exploited to form hydrogel biomaterials via bioorthogonal SPAAC chemistry.

during gelation, the maximal extent of material response can be precisely controlled.

End-modified protein crosslinkers are prepared through a novel orthogonal pair of chemoenzymatic modifications (Figure 1c). N-terminal labeling is achieved by *N*-myristoyl transferase (NMT), which promotes cotranslational fatty acylation on proteins bearing the “GXXXS/T” signature sequence (where X is any amino acid). NMT tolerates many synthetic analogs of its natural myristic acid substrate; enzymatic modification with 12-azidododecanoic acid (12-ADA, Method S5, Supporting Information) yields site-specific installation of azide functionality at the N-terminus.<sup>[44–46]</sup> To append bio-orthogonal handles onto the C-terminus of proteins, we exploit a versatile sortase-mediated transpeptidation reaction.<sup>[47,48]</sup> *Staphylococcus aureus* sortase A is a calcium-assisted transpeptidase that catalyzes the cleavage of a C-terminal sorting signal “LPXTG” with the concomitant amide linkage of a polyglycine probe and the target protein. “Sortagging” with an azide-bearing oligoglycine permits efficient C-terminal installation of azido functionality (Method S6, Supporting Information). Though both NMT and sortase have each been used in isolation to introduce a single reactive azide onto either the N- or C-terminus of a protein,<sup>[44–46,49]</sup> their combined usage has not been demonstrated in literature. In fact, modification of a single protein by multiple chemoenzymatic reactions has not yet been established. Here, we demonstrate that recombinant proteins bearing both enzymatic recognition sequences can be readily prepared through standard molecular cloning and expression techniques. As chemoenzymatic transformations proceed with

exceptionally high labeling efficiencies,<sup>[50]</sup> we hypothesized that uniform populations of dually functionalized protein-based material crosslinkers could be created from virtually any monomeric or fused species, and that they could function uniquely as macromolecular precursors for the controlled step-growth polymerization of protein–polymer hydrogels.

Having identified a strategy to create stiffness-cyclable hydrogels using dually modified responsive proteins, we focused our initial efforts on calmodulin (CaM), a calcium-sensitive protein whose stimuli sensitivity has been previously utilized to make dynamic materials.<sup>[24,25]</sup> Taking lead from an expansive body of genetically encoded calcium sensors,<sup>[51–54]</sup> we created a fusion of CaM and the M13 peptide fragment of myosin light chain kinase that could be dually modified for gel crosslinking (Method S7, Supporting Information). When  $\text{Ca}^{2+}$  is present, CaM undergoes a conformational change that permits high-affinity binding with M13; when the ion is chelated away, CaM structure and intramolecular association relaxes (Figure 2a). Following expression and modification by NMT and sortase, the end-modified  $\text{N}_3\text{-CaM-M13-N}_3$  complex was obtained in good yield ( $\approx 5 \text{ mg L}^{-1}$  culture, nonoptimized expression, Method S8, Supporting Information). Whole-protein mass spectrometry revealed exceptionally high sample purity and quantitative functionalization at both termini (Figure 2b, Method S9 and Tables S1 and S2 (Supporting Information)); the observed mass for  $\text{N}_3\text{-CaM-M13-N}_3$  (22 807 Da) correlated well with its expected value (22 805 Da). Far-UV circular dichroism confirmed responsiveness of the complex to calcium (Figure 2c), consistent with similar analysis performed on purified CaM,<sup>[55]</sup>

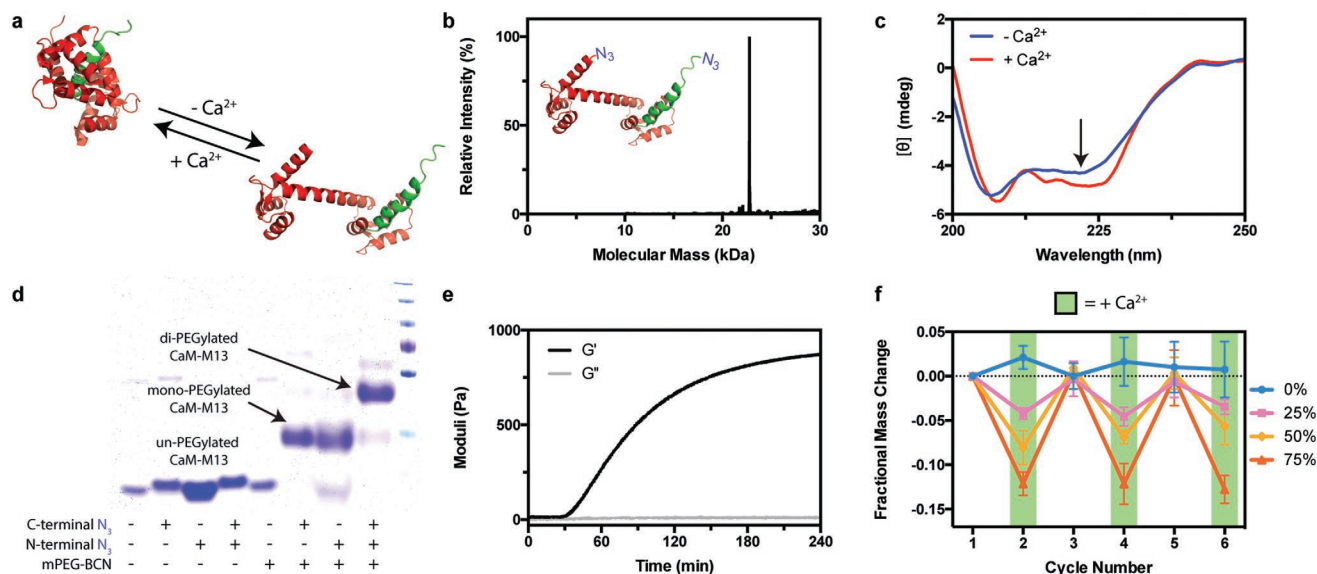


**Figure 2.** Calcium-responsive gels based on CaM–M13 intramolecular binding. a) Calmodulin (CaM, shown in red) reversibly associates with fusion partner M13 (shown in green) in a calcium-dependent manner. b) Whole-protein mass spectrometry reveals that end-functionalized  $\text{N}_3\text{-CaM-M13-N}_3$  is generated with high purity. c) Far-UV circular dichroism indicates that  $\text{N}_3\text{-CaM-M13-N}_3$  undergoes stimuli-dependent conformational changes in the presence and absence of  $\text{Ca}^{2+}$ . Decreased ellipticity at 222 nm (denoted with an arrow) indicates increased  $\alpha$ -helical content of the protein when  $\text{Ca}^{2+}$  is bound. d) SDS-PAGE gel shift assays with a monofunctionalized methoxy-PEG–bicyclononyne indicate that azides can be selectively and quantitatively introduced at both protein termini, and that installed azides remain active and accessible for SPAAC chemistry. e) Reaction of PEG–tetraBCN ( $2 \times 10^{-3} \text{ M}$ ),  $\text{N}_3\text{-PEG-N}_3$  ( $2 \times 10^{-3} \text{ M}$ ), and  $\text{N}_3\text{-CaM-M13-N}_3$  ( $2 \times 10^{-3} \text{ M}$ ), as monitored through dynamic time-sweep rheological analysis, yields robust gels on a timescale that is appropriate for cell encapsulation. f) CaM–M13 gels exhibit reversible swelling, as quantified by fractional mass change, in the presence and absence of  $\text{Ca}^{2+}$ . Total responsiveness scales with protein crosslinker content (0, 25, 50, 75 mol%  $\text{N}_3\text{-CaM-M13-N}_3$ , with the balance comprised of  $\text{N}_3\text{-PEG-N}_3$ ).

where  $\alpha$ -helical content increases upon  $\text{Ca}^{2+}$  binding, as indicated by decreasing ellipticity at 222 nm.<sup>[56]</sup> To verify that the introduced azides were functionally accessible and maintained reactivity by SPAAC, we utilized a sodium dodecyl sulfate polyacrylamide gel electrophoresis (SDS-PAGE) gel shift assay<sup>[57]</sup> involving C-/N-terminal PEGylation by BCN-monofunctionalized methoxy-PEG (mPEG-BCN,  $M_n \approx 10$  kDa, Method S10, Supporting Information) (Figure 2d); the near-complete disappearance of the starting protein band, accompanied by the simultaneous appearance of a new band upshifted by the average molecular weight of the correct number of PEG chains (0, 1, or 2, depending on condition), indicates the ability to install reactive azides site specifically onto CaM-M13 proteins using NMT and/or sortase. Collectively, these results demonstrate the successful generation of a bioresponsive fusion protein-based crosslinker, as well as the first utilization of two different chemoenzymatic reactions to modify a single recombinant protein.

Calcium-responsive hydrogel networks were formed based on the SPAAC reaction of PEG-tetraBCN ( $2 \times 10^{-3}$  M),  $\text{N}_3$ -PEG- $\text{N}_3$  ( $2 \times 10^{-3}$  M), and  $\text{N}_3$ -CaM-M13- $\text{N}_3$  ( $2 \times 10^{-3}$  M). Dynamic time-sweep rheological experiments indicated gelation  $\approx 30$  min after mixing, estimated by the crossover point between the elastic ( $G'$ ) and storage moduli ( $G''$ ), and a final  $G'$  of  $920 \pm 50$  Pa and  $G''$  of  $15 \pm 5$  Pa at  $t \approx 5$  h (Figure 2e). To assess changes in network composition in response to free-ion treatment, we examined cycled changes of mass swelling ratios in the presence or absence of calcium. When incubated with  $\text{Ca}^{2+}$ , materials crosslinked with 50 mol% CaM-M13 exhibit a  $6.8 \pm 1.5\%$  decrease in swollen gel mass, reflecting the overall network constriction and a net loss in equilibrium water retention that accompanies CaM association with M13 (Figure 2f). Varying the ratio of  $\text{N}_3$ -PEG- $\text{N}_3$  to  $\text{N}_3$ -CaM-M13- $\text{N}_3$  while keeping their total concentration constant ( $4 \times 10^{-3}$  M) gave materials with scaled responsiveness; gels formed with 0, 25, 50, and 75 mol% CaM-M13, respectively, exhibited  $1.5 \pm 2.3\%$ ,  $4.1 \pm 0.9\%$ ,  $6.8 \pm 1.5\%$ , and  $12.4 \pm 1.7\%$   $\text{Ca}^{2+}$ -promoted decrease in mass swelling. Based on Flory-Rehner polymer network theory,<sup>[58]</sup> which predicts that swelling ratio ( $Q$ ) of highly swollen materials scales with crosslinking density ( $\rho_x$ ) as  $Q \sim \rho_x^{-3/5}$  and shear moduli ( $G$ ) as  $G \sim \rho_x^{6/5}$ ,  $\text{Ca}^{2+}$ -promoted decrease in swelling observed for the 25, 50, and 75 mol% CaM-M13, respectively, results in a  $8.7 \pm 2.0\%$ ,  $15 \pm 3.8\%$ , and  $30 \pm 4.8\%$  relative gel stiffening. In all cases, initial hydrogel mass was restored following egtazic acid (EGTA)-mediated chelation of free  $\text{Ca}^{2+}$ . Alternate treatments of  $\text{Ca}^{2+}$  and EGTA gave rise to reproducible material cyclability. We expect that the extent of hydrogel stiffening could be further tuned by varying the distance change that accompanies the fusion protein's conformational switch, which could be accomplished by varying molecular weight of multiarm PEG or through addition of spacers between protein binding partners.

Though the CaM-M13 system proved useful in validating our overall fusion protein-based approach, its utility in probing cell fate response to cyclic stiffening is limited: 1) alterations to network mechanics rely on slow molecular diffusion events, preventing rapid control over material switchability; 2) calcium signaling is involved in almost all aspects of cellular life,<sup>[59]</sup> rendering it impossible to alter network parameters without

also perturbing biological function; and 3) spatial control over network mechanics is not readily possible. To address each of these limitations, we identified the photoswitchable LOV2-J $\alpha$  binding pair for use as a stimuli-responsive fusion protein. Recently popularized by the optogenetics community,<sup>[60-63]</sup> the light, oxygen, and voltage sensing domain 2 (LOV2) is a plant-derived photoreceptor protein with a high binding affinity toward the C-terminal J $\alpha$  helix.<sup>[64]</sup> In the presence of blue light ( $\lambda = 470$  nm), LOV2 initiates a photochemical reaction with a flavin mononucleotide chromophore (FMN), forming a covalent linkage between FMN and a critical cysteine residue on LOV2, that results in a displacement of the J $\alpha$  domain and a large conformational shift (end-to-end changes estimated to be on the order of tens of Angstroms). This change occurs rapidly in response to low levels of blue light, and reverses quickly in the dark (Figure 3a). As cells are considered fully tolerant to light with wavelengths  $\geq 365$  nm,<sup>[65,66]</sup> there is no concern over UV-induced DNA damage when visible light sources are employed. We anticipated that utilization of LOV2-J $\alpha$  as a gel crosslinker would enable unique photoreversible and spatiotemporal control over hydrogel stiffness in the presence of live cells.

Expression of  $\text{N}_3$ -LOV2-J $\alpha$ - $\text{N}_3$  yielded a pure species with quantitative functionalization, as confirmed by whole-protein mass spectrometry (Figure 3b, Methods S7-S9 and Tables S1 and S2 (Supporting Information)); the observed mass for  $\text{N}_3$ -LOV2-J $\alpha$ - $\text{N}_3$  (18 841 Da) correlated well with its expected value (18 848 Da). The diazide protein exhibited the near-instantaneous shift in absorbance in response to blue light ( $\lambda = 470$  nm), followed by a rapid dark recovery ( $t_{1/2} = 12 \pm 5$  s, high standard deviation based on equipment sampling frequency limitations) characteristic to the unmodified LOV2,<sup>[67]</sup> indicating that the protein is properly folded and that the FMN chromophore survives purification (Figure 3c and Figure S1 (Supporting Information)). Gel shift assays performed with mPEG-BCN confirmed that azides affixed at both the N- and C-termini of LOV2-J $\alpha$  were accessible and maintained reactivity, as well as successful generation of a light-responsive protein-based crosslinker (Figure 3d).

Photoswitchable gels were formed by reaction of PEG-tetraBCN ( $2 \times 10^{-3}$  M),  $\text{N}_3$ -PEG- $\text{N}_3$  ( $2 \times 10^{-3}$  M), and  $\text{N}_3$ -LOV2-J $\alpha$ - $\text{N}_3$  ( $2 \times 10^{-3}$  M). In situ rheometry indicated that hydrogels formed on similar timescales and with comparable mechanics as CaM-M13-based materials. Photorheometry studies revealed that fully formed gels exhibited rapid softening ( $t_{1/2} = 0.9 \pm 0.2$  s) in response to mild visible light ( $\lambda = 470$  nm,  $10$  mW  $\text{cm}^{-2}$ ) (Figure 3e). Varying the ratio of  $\text{N}_3$ -PEG- $\text{N}_3$  to  $\text{N}_3$ -LOV2-J $\alpha$ - $\text{N}_3$  while keeping their total concentration constant ( $4 \times 10^{-3}$  M) gave materials with scaled responsiveness; gels formed with 0, 25, 50, and 75 mol% LOV2-J $\alpha$ , respectively, exhibited  $0.0 \pm 0.1\%$ ,  $4 \pm 1\%$ ,  $8 \pm 1\%$ ,  $15 \pm 1\%$  photomediated moduli deflation. The softened state was retained until light exposure was ceased, upon which full material recovery was observed ( $t_{1/2} = 35 \pm 1$  s). As expected, the timescale for gel recovery is similar but slightly slower (approximately threefold) than that of LOV2's covalent separation from FMN, as presumably some time is required for LOV2-J $\alpha$  binding partners to reassociate following LOV2's conformational change. Characteristic timescales for material softening

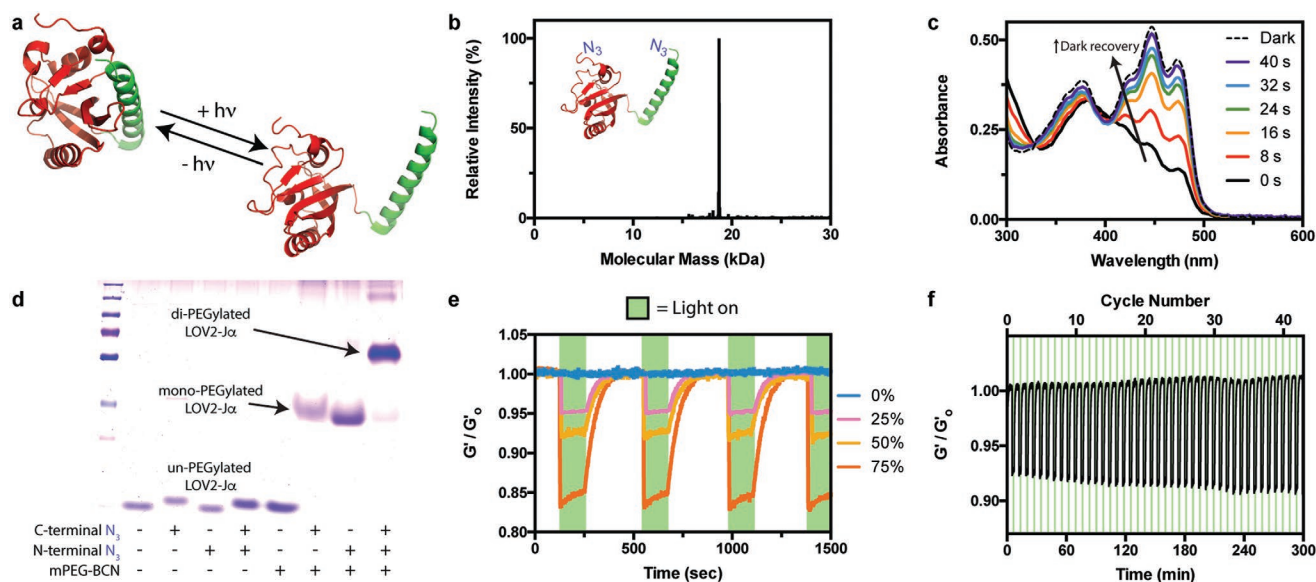


**Figure 3.** Moduli-switchable hydrogels based on LOV2–J $\alpha$  intramolecular photodissociation. a) Light, oxygen, and voltage sensing domain 2 (LOV2, shown in red) undergoes reversible dissociation with the C-terminal J $\alpha$  helix (green) in response to blue light ( $\lambda = 470$  nm). This conformational change is reversed under dark conditions. b) End-functionalized N<sub>3</sub>–LOV2–J $\alpha$ –N<sub>3</sub> is obtained in high purity, as indicated by whole-protein mass spectrometry. c) Dark recovery photokinetic analysis of N<sub>3</sub>–LOV2–J $\alpha$ –N<sub>3</sub> immediately following photomediated protein dissociation. Near-complete recovery is observed after 40 s, as indicated by curve similarity with “dark” samples never exposed to light. d) Azides can be selectively and quantitatively installed to LOV2–J $\alpha$  termini, as indicated by SDS-PAGE gel shift assays with a monofunctionalized methoxy-PEG–bicyclononyne. Bioorthogonal handles remain accessible and reactive via SPAAC. e) LOV2–J $\alpha$ -based gels exhibit repeated and reversible changes in elastic moduli in response to blue light ( $\lambda = 470$  nm, 10 mW cm<sup>-2</sup>), as determined by in situ photorheometry. Total responsiveness scales with protein crosslinker content (0, 25, 50, 75 mol% N<sub>3</sub>–LOV2–J $\alpha$ –N<sub>3</sub>, with the balance comprised of N<sub>3</sub>–PEG–N<sub>3</sub>). f) LOV2–J $\alpha$  gel stiffness can be rapidly cycled with negligible material fatigue, shown here for gels comprised of 50 mol% protein crosslinker.

and stiffening were statistically indistinguishable for each LOV2–J $\alpha$  gel composition. We note that LOV2’s temporary “bleaching” following exposure at wavelengths used to trigger its conformational change (Figure 3c) minimizes light attenuation and enables rapid modulation of relatively thick materials. In comparison with reported gels that soften through photoinduced intermolecular dissociation, particularly those employing high concentrations of photoactive moieties with large molar absorptivity,<sup>[28,34–36]</sup> LOV2–J $\alpha$  gels can be uniformly softened throughout the bulk material without inducing surface erosion. By shuttering light exposure to gels, full cyclability was obtained for all materials. Negligible material fatigue was observed for 50 mol% LOV2–J $\alpha$  gels cycled >40 times over 5 h (Figure 3f and Figure S2 (Supporting Information)). Such moduli cyclability, made possible by rapid molecular rearrangement events, has not been demonstrated previously with any other biocompatible system.

In addition to providing unprecedented temporal and cycled control over matrix properties, directed light exposure can be used to confine LOV2–J $\alpha$  gel softening to user-defined physical locations (Figure 4a). As the fast gel transition times and light responsiveness prevent localized mechanical characterization by many conventional techniques (e.g., atomic force microscopy, nanoindentation, microrheology), we took advantage of the distinct visible color shift that accompanies LOV2 photoactivation to monitor local stiffness changes within gels (Figure 3c); stiffer materials where LOV2 is noncovalently bound to FMN but is associated with J $\alpha$  appear yellow under ambient light, while softer substrates in which LOV2 is covalently bound

to FMN and dissociated from J $\alpha$  are visually clearer. Image analysis of gel color following blue light flood exposure ( $\lambda = 470$  nm, 1 mW cm<sup>-2</sup>, 30 s) revealed a dark recovery rate ( $t_{1/2} = 14 \pm 3$  s, Figure 4b) consistent with in-solution LOV2–J $\alpha$  analysis. Patterned regions of gel softening were created by traditional photolithographic techniques, whereby collimated light was shone through a photomask onto the surface of an optically thin sample. Gels were imaged before and after photopatterning; temporary changes in gel color and moduli matched masked-defined shapes (Figure 4c and Movies S1–S3 (Supporting Information)). Upon complete stiffness recovery, sequential patterning was performed using the same gel and a different photomask. Results highlight the platform’s unique spatiotemporal control over material compliance as well as its reversibility, where patterning can be repeated many times over to soften different material regions as desired. Furthermore, laser-scanning lithographic technique enables gels to be reversibly softened with micrometer-scale features that approach the size of single cells (Figures S3 and S4, Supporting Information).

Using our reversibly compliant LOV2–J $\alpha$  hydrogels, we sought to establish the first understanding concerning the role of cyclic mechanical loading on myofibroblast activation in 3D. Upon injury, fibroblasts transdifferentiate into myofibroblasts that promote ECM remodeling.<sup>[68]</sup> This activation can be regulated chemically through cytokine stimulation as well as through physical interactions with matrix substrates, and is associated with increased smooth muscle  $\alpha$ -actin ( $\alpha$ SMA) and periostin (*Postn*) gene expression.<sup>[69]</sup> Though material stiffness and cyclic stretching of flexible 2D materials (which have

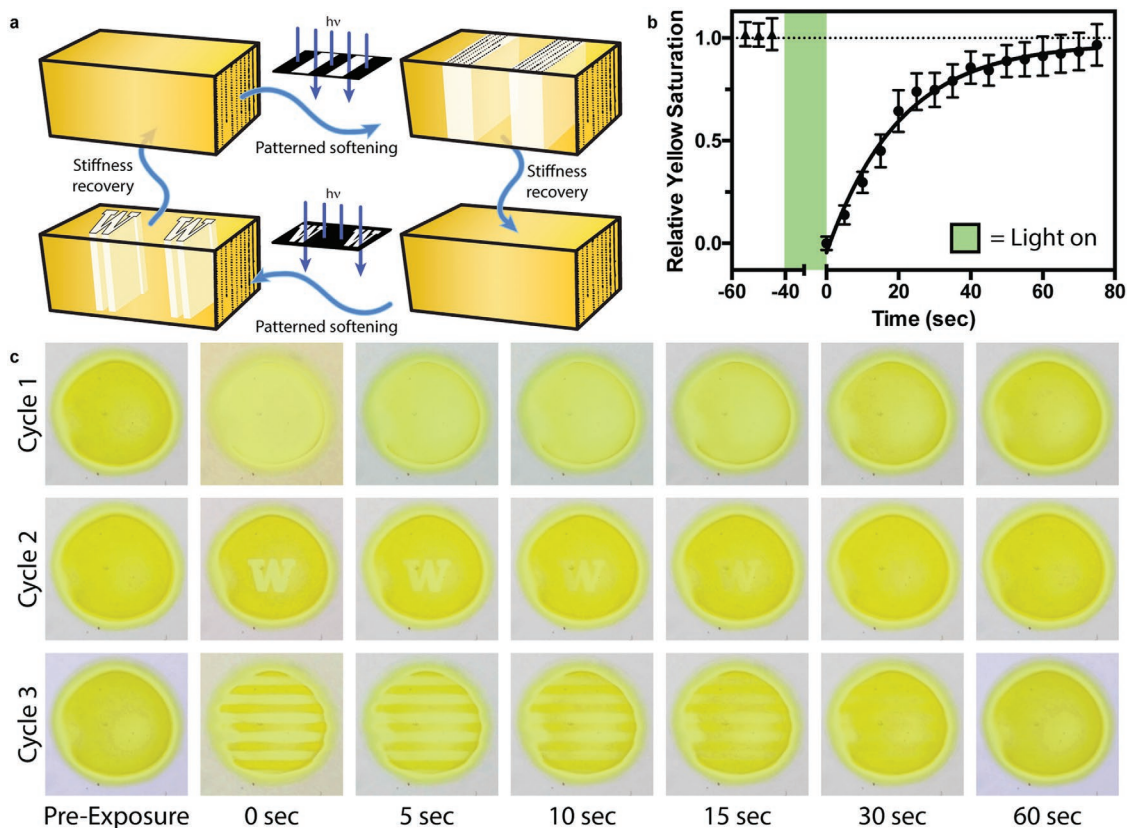


**Figure 4.** Photoreversible and spatiotemporal control over LOV2- $\alpha$  gel mechanics. a) Stiffness-patterned hydrogels are readily generated upon masked exposure to blue light ( $\lambda = 470$  nm). In the dark, these materials rapidly reset to a uniformly stiff gel. The patterning process is repeatable and scalable. b) LOV2- $\alpha$  gels exhibit state-dependent color profiles; stiffer gels appear yellow under ambient light, while softer substrates are visually clearer. Image analysis of hydrogel color following flood light exposure ( $\lambda = 470$  nm,  $1 \text{ mW cm}^{-2}$ , 30 s) reveals fast dark recovery. Yellow saturation of gels over time is normalized between values preceding and immediately following light exposure (1 and 0, respectively). c) Mask-based photolithography is used to confine LOV2- $\alpha$  gel softening to user-defined physical locations. Following flood light exposure and full recovery (Cycle 1), a single gel was softened in regions corresponding to the “Boundless W” logo of the University of Washington (Cycle 2). After returning to a uniform stiffness, the gel was softened in interspaced line patterns prior to complete recovery (Cycle 3). Gel diameter  $\approx 1$  cm, thickness  $\approx 200$   $\mu\text{m}$ .

not yet been shown to support cell encapsulation) can drive changes in enhanced activation,<sup>[70,71]</sup> material limitations have prevented investigation of the effects of dynamic mechanical loading on 3D myofibroblast transformation (Figure 5a). To probe these effects, NIH/3T3 fibroblasts were encapsulated ( $5 \times 10^6$  cells  $\text{mL}^{-1}$ ) in 50 mol% LOV2- $\alpha$  hydrogels (a composition initially chosen to minimize protein consumption while still yielding materials with robust mechanical tunability) and cultured for 48 h under three different material conditions: 1) continuous flood exposure ( $\lambda = 470$  nm,  $1 \text{ mW cm}^{-2}$ ) giving rise to softer gels; 2) dark culture yielding comparatively stiff materials; and 3) shuttered light exposure (1 min on, 4 min off), providing gels with cycled compliance (Figure 5b). The extent of softening ( $\approx 8\%$  of initial moduli) and the dark material recovery rate ( $t_{1/2} \approx 35$  s) were similar for gels containing encapsulated cells in culture media (Figure 5b) or simply swollen in phosphate buffered saline (PBS) (Figure 3e,f), indicating that the system functions equally well in the presence or absence of complex biological components. High cell viability ( $\approx 95\%$ ) was observed in all conditions, demonstrating the overall cyto-compatibility of gel formation and subsequent photomechanical material alterations (Figure 5c and Figure S5 (Supporting

Information)). To determine the effects of each culture condition on fibroblast-to-myofibroblast differentiation, we quantified associated changes in luciferase activity of fibroblasts transfected with an  $\alpha\text{SMA}$ -luciferase transcriptional reporter plasmid<sup>[72]</sup> (Figure 5d). As expected, significant changes in  $\alpha\text{SMA}$  transcriptional activity was observed for cells cultured between “stiff” and “soft” materials. Interestingly, myofibroblast activation was further enhanced within reversibly stiffening gels. This activating effect was reconfirmed by Western blot analysis of untransfected fibroblasts for expression of  $\alpha\text{SMA}$  relative to housekeeper protein glyceraldehyde 3-phosphate dehydrogenase (Figure S6, Supporting Information). We further confirmed the observed effects using fibroblasts transfected with a *Postn*-luciferase transcriptional reporter plasmid,<sup>[72]</sup> which acts as an additional transcriptional surrogate of myofibroblast differentiation. These findings are further substantiated by recent studies in 2D, where fibroblasts seeded on silicon membranes and subjected to cyclic stretching exhibited enhanced activation.<sup>[73]</sup> Observed differences in 3D fibroblast transdifferentiation motivate further investigation, whereby differences in anisotropic cyclic mechanical loading are expected to play a large role in regulating powerful, yet largely unexplored, biological phenomena.

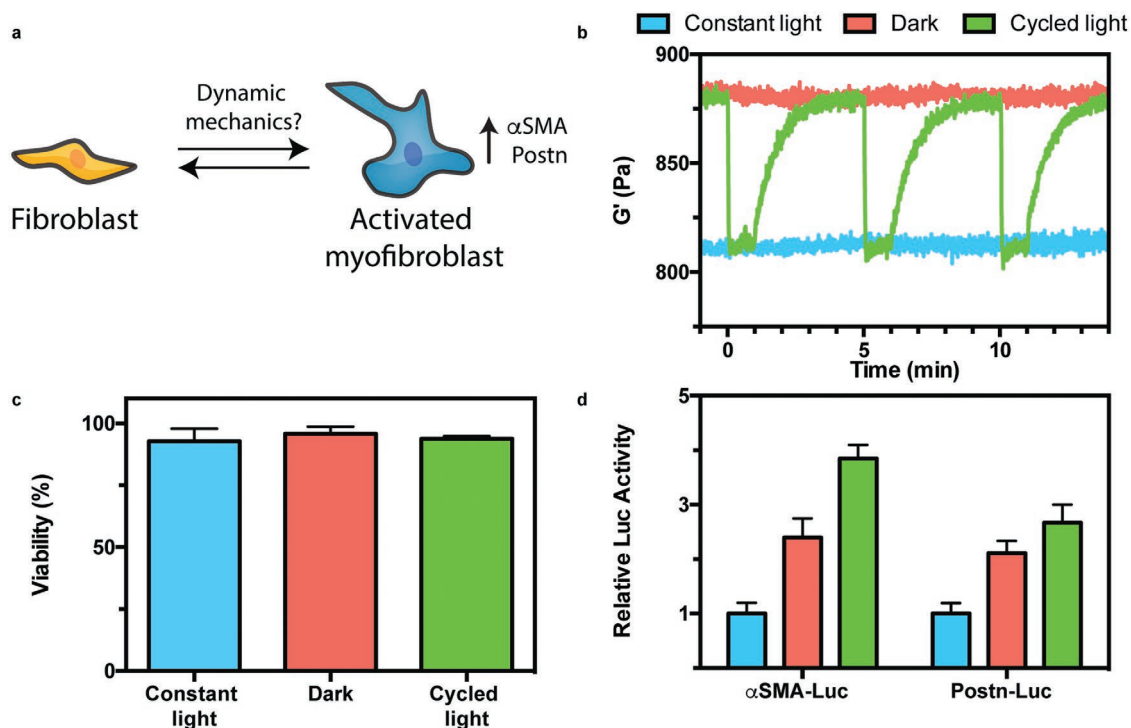


**Figure 5.** Cyclic mechanical loading drives myfibroblast activation. a) Fibroblasts transdifferentiate into myfibroblasts in response to both chemical and physical stimulation. The role of dynamic mechanics in this process remains largely unknown, particularly in 3D. b) NIH/3T3 fibroblasts were cultured within LOV2- $\alpha$  hydrogels, each exhibiting a different time-dependent stiffness profile. Dark culture gives stiffer gels; continuous flood exposure ( $\lambda = 470$  nm,  $1$  mW  $\text{cm}^{-2}$ ) yields comparatively soft gels; and shuttered light exposure (1 min on, 4 min off) provides gels with cycled compliance. In situ rheometric analysis was performed on cell-laden gels with 50% LOV2- $\alpha$  crosslinker in culture media. c) LIVE/DEAD staining at 48 h of cells encapsulated within this material reveals a predominantly viable population for all material treatment conditions. d) Fibroblast-to-myfibroblast transformation varies significantly with stiffness dynamics, as indicated by transcriptional activity analysis of NIH/3T3s transfected with an  $\alpha$ SMA-luciferase and *Postn*-luciferase promoter plasmids.

The results described here illustrate a generalizable strategy to create biomaterials whose mechanics can be cycled in response to user-defined inputs. Through the first demonstrated dual-chemoenzymatic modification of a recombinant protein, we create fusion species exhibiting stimuli-dependent intramolecular association that can be used as the basis for step-growth polymerization of gels. Implementation of the technique with the photoactive LOV2 protein yielded unprecedented reversible and spatiotemporal control over network dynamics, newly capturing critical aspects of the cellular micro-environment. These unique materials were used to investigate 3D biological response to cyclic loading, an important aspect of native ECM that has not been previously replicated in vitro. We expect that this approach will provide a new dimension to the growing field of mechanobiology, and will prove useful in the creation of a wide variety of protein-based and stimuli-responsive materials for tissue engineering, drug delivery, and many other applications.

## Experimental Section

**Synthesis and Purification of End-Functionalized Stimuli-Responsive Fusion Proteins:** Plasmids encoding for CaM-M13 and LOV2- $\alpha$ , flanked with an N-terminal NMT- and a C-terminal sortase-recognition peptide sequence (MGNEASYPL and LPETG, respectively), were

constructed using standard cloning techniques (Method S7, Supporting Information) and each cotransformed with those encoding for NMT/methionine aminopeptidase (Met-AP) into BL21(DE3) *Escherichia coli* (Thermo Fisher). Successful cotransformants were grown at 37 °C in lysogeny broth containing ampicillin (100  $\mu\text{g mL}^{-1}$ ) and kanamycin (50  $\mu\text{g mL}^{-1}$ ). After reaching an optical density of 0.6 ( $\lambda = 600$  nm), isopropyl  $\beta$ -D-1-thiogalactopyranoside was added (final concentration of  $0.5 \times 10^{-3}$  M) to induce expression. Expression was carried out with or without 12-ADA (final concentration of 140  $\text{mg L}^{-1}$ , Method S5, Supporting Information) overnight under reduced temperature (18 °C). Cells were harvested via centrifugation and lysed by sonication. Clarified lysate was loaded onto HisPur Ni-NTA resin (Thermo Fisher), which was washed (20  $\times 10^{-3}$  M Tris, 50  $\times 10^{-3}$  M NaCl, 20  $\times 10^{-3}$  M imidazole) to remove unbound proteins. Following treatment of the resin with triglycine or an azide-containing polyglycine probe (20 $\times$ , 4 h, 37 °C), sortagged proteins were eluted and purified by dialysis (molecular weight cutoff, MWCO  $\approx 10$  kDa). Protein identity and purity was confirmed by liquid chromatography-tandem mass spectrometry, SDS-PAGE, and gel shift analysis. Ultraviolet absorption ( $\lambda = 280$  nm) and bicinchoninic acid assays were used to determine protein concentrations prior to use. Purified proteins remained stable for several weeks, based on their ability to form responsive gels, when kept refrigerated (4 °C) in PBS (pH = 7.4). Complete experimental details are given in Methods S7–S9 (Supporting Information).

**Assessing  $\text{Ca}^{2+}$ -Dependent Conformational Changes of CaM-M13:** Far-UV circular dichroism (CD) measurements were performed on a Jasco 720 CD spectrophotometer (1 mm path length, quartz cuvette) purged with nitrogen gas from 200  $\leq \lambda \leq 250$  nm (scan rate = 100  $\text{nm min}^{-1}$ ). Spectra were recorded for  $\text{N}_3$ -CaM-M13- $\text{N}_3$  (25  $\mu\text{g mL}^{-1}$ ) in buffer (20  $\times 10^{-3}$  M Tris, 30  $\times 10^{-3}$  M KCl) supplemented with either calcium

( $1 \times 10^{-3}$  M CaCl<sub>2</sub>) or EGTA ( $1 \times 10^{-3}$  M), and were normalized against protein-free controls.

**Determining Extent of Protein Chemoenzymatic Modifications:** To assess the ability for sortase and NMT to generate homogenous protein samples with quantitative reactivity, an SDS-PAGE gel shift assay was performed for each purified protein species (CaM–M13, CaM–M13–N<sub>3</sub>, N<sub>3</sub>–CaM–M13, N<sub>3</sub>–CaM–M13–N<sub>3</sub>, LOV2–J $\alpha$ , LOV2–J $\alpha$ –N<sub>3</sub>, N<sub>3</sub>–LOV2–J $\alpha$ , N<sub>3</sub>–LOV2–J $\alpha$ –N<sub>3</sub>). Following reaction (24 h at 37 °C) with mPEG–BCN (100x) in buffer (20  $\times 10^{-3}$  M Tris, 50  $\times 10^{-3}$  M NaCl, 20  $\mu$ L), denatured proteins (1  $\mu$ g) were separated electrophoretically in polyacrylamide gels and visualized by Coomassie Brilliant Blue (Thermo Fisher) staining.

**Step-Growth Polymerization of Protein–Polymer Hydrogels:** Protein–polymer hydrogels were formed by SPAAC between PEG–tetraBCN (2  $\times 10^{-3}$  M) and diazide crosslinking species in PBS (pH = 7.4). The diazide crosslinker mixture (4  $\times 10^{-3}$  M total) was comprised of modified fusion proteins (N<sub>3</sub>–CaM–M13–N<sub>3</sub> or N<sub>3</sub>–LOV2–J $\alpha$ –N<sub>3</sub>, 0–3  $\times 10^{-3}$  M) and a balance of N<sub>3</sub>–PEG–N<sub>3</sub> (1  $\times 10^{-3}$ –4  $\times 10^{-3}$  M) to yield gels with 0, 25, 50, or 75 mol% protein crosslinker content. Upon component mixing, gelation was permitted to proceed for 2 h between Rain-X-treated glass slides (500  $\mu$ m spacing) prior to slide separation and subsequent equilibration in PBS. For cell-laden gel formation, PEG–tetraBCN was prereacted (1 h) with N<sub>3</sub>–GRGDS–NH<sub>2</sub> peptide (0.5  $\times 10^{-3}$  M final in-gel concentration, Method S11, Supporting Information) prior to mixture with crosslinking species and cells in culture media. Protein–polymer gels based on CaM–M13 and LOV2–J $\alpha$  each remained fully stable after two weeks of storage in cell culture media at 37 °C (Figure S7, Supporting Information), indicating that the PEGylated protein crosslinkers are not particularly prone to hydrolytic or enzymatic degradation.

**Mechanical Testing of Protein–Polymer Gels:** In situ rheological experiments were performed on optically thin (50  $\mu$ m) protein–polymer gels formed between parallel quartz plates (8 mm diameter). The rheometer (Discovery HR-2, TA Instruments) was outfitted with a collimated blue light source ( $\lambda$  = 470 nm, 10 mW cm<sup>-2</sup>, Thorlabs) whose exposure was shuttered with an automated controller (NEARPOW) in experiments investigating the light-responsiveness of LOV2–J $\alpha$  gels (Figure S8, Supporting Information). The storage and loss moduli ( $G'$  and  $G''$ , respectively) were measured by oscillatory rheology at constant strain (1%) and frequency (1 rad s<sup>-1</sup>), conditions determined to fall within the linear viscoelastic region of the gels. A thin coating of mineral oil around gel perimeter was employed to prevent evaporation during measurements.

**Ca<sup>2+</sup>-Dependent Changes in CaM–M13 Gel Swelling:** CaM–M13 gels (0–75 mol% protein content) were equilibrated in buffer (20  $\times 10^{-3}$  M 4-(2-hydroxyethyl)-1-piperazineethanesulfonic acid, 50  $\times 10^{-3}$  M NaCl), alternating between that supplemented with CaCl<sub>2</sub> (1  $\times 10^{-3}$  M, 4 h) or EGTA (1  $\times 10^{-3}$  M, 8 h) to cycle gel swelling. Fractional mass changes, defined as the change in swollen gel mass relative to that of the initial swollen gel, were determined for each gel type after full equilibration and immediately preceding buffer exchange.

**Spatiotemporal Control of Reversible Gel Softening:** 50 mol% LOV2–J $\alpha$  gels were exposed to collimated blue light ( $\lambda$  = 470 nm, 1 mW cm<sup>-2</sup>, 30 s) through a patterned chrome photomask (Photo Sciences, Inc.). Gels were visualized before and immediately after light exposure through time-lapse videography using a digital camera (Nikon). Image analysis of gel color following flood light exposure ( $\lambda$  = 470 nm, 1 mW cm<sup>-2</sup>, 30 s) was performed (ImageJ) to determine yellow saturation content (interval = 5 s).

**3T3 Fibroblast Cell Culture:** Unmodified and transfected NIH 3T3 fibroblast cells were cultured in Dulbecco's modified Eagle's medium supplemented with fetal bovine serum (10%, Corning) and penicillin/streptomycin (1%, Corning) in a 5% CO<sub>2</sub> atmosphere at 37 °C. Culture medium was changed every two to three days, and cells were passaged at  $\approx$ 90% confluency. Following trypsinization, fibroblasts were encapsulated (5  $\times 10^6$  cells mL<sup>-1</sup>) in 50 mol% LOV2–J $\alpha$  gels modified with N<sub>3</sub>–GRGDS–NH<sub>2</sub> (0.5  $\times 10^{-3}$  M, Method S11, Supporting Information).

**Cell Responses to Reversible Matrix Stiffness Modulation:** NIH/3T3 fibroblasts were transfected with either an  $\alpha$ SMA–luciferase or a *Postn*–luciferase promoter plasmid.<sup>[72,74]</sup> Transfection conditions

(1.66  $\mu$ g DNA  $\mu$ L<sup>-1</sup> Lipofectamine 3000) were selected so as to maximize transfection efficiency (here, 65%) while retaining cell morphology and health. Transfected NIH/3T3 fibroblasts were encapsulated (5  $\times 10^6$  cells mL<sup>-1</sup>) in 50 mol% LOV2–J $\alpha$  hydrogels in three polystyrene 24-well cell culture plates (Corning) under three different material conditions: 1) continuous flood exposure ( $\lambda$  = 470 nm, 1 mW cm<sup>-2</sup>) giving rise to softer gels; 2) dark culture yielding comparatively stiff materials; and 3) shuttered light exposure (1 min on, 4 min off). After cultured maintenance of these light exposure conditions for 48 h, samples were ground with a mortar and pestle and resuspended in lysis buffer (50  $\mu$ L, 1% Triton X-100, 100  $\times 10^{-3}$  M Tris–HCl, 2  $\times 10^{-9}$  M ethylenediaminetetraacetic acid, 2  $\times 10^{-3}$  M dithiothreitol) prior to luciferase analysis (Pierce Firefly Luciferase Glow Assay, Thermo Fisher). Luciferase activity was measured in triplicate for each material condition.

## Supporting Information

Supporting Information is available from the Wiley Online Library or from the author.

## Acknowledgements

The authors recognize and thank Dr. A. Nelson (University of Washington, UW) for generously providing access to their rheometer, Dr. L. Newman and Dr. R. Kahn (Emory University) for gifting the hNMT1 with Met-AP plasmid,<sup>[75]</sup> as well as Dr. R. Warden-Rothman and Dr. A. Tsourkis (University of Pennsylvania) for providing the pSTEPL plasmid.<sup>[76]</sup> Yellow Cameleon-Nano15/pBig was a gift from Takeharu Nagai (Addgene plasmid # 51962). pTriEx-PA-Rac1 was a gift from Klaus Hahn (Addgene plasmid # 22024). The authors thank B. Badeau for assistance in synthesizing N<sub>3</sub>–OSu and Fmoc–Lys(N<sub>3</sub>)–OH, as well as S. Adelmund for providing BCN–OSu. The authors gratefully acknowledge support from S. Edgar at the UW Mass Spectrometry Center, the NIH and N. Peters at the UW W. M. Keck Microscopy Center (Grant No. S10 OD016240), as well as from D. Wise and N. Bragg (UW Marketing and Communications) for their assistance with visually analyzing spatiotemporal changes in LOV2–J $\alpha$  gel mechanics. This work was supported by a UW Faculty Startup Grant (C.A.D.), an Institute for Stem Cell & Regenerative Medicine Innovation Pilot Award (C.A.D.), a CAREER Award (DMR 1652141, C.A.D.) from the National Science Foundation, and a Pathway to Independence Award (Grant No. K99/R00 HL119353-01, J.D.) from the National Institutes of Health.

## Conflict of Interest

The authors declare no conflict of interest.

## Keywords

4D biology, biomaterials, hydrogels, photochemistry, protein engineering

Received: August 8, 2018

Revised: September 5, 2018

Published online: October 12, 2018

[1] D. E. Ingber, *FASEB J.* **2006**, *20*, 811.

[2] A. J. Engler, S. Sen, H. L. Sweeney, D. E. Discher, *Cell* **2006**, *126*, 677.

[3] C. C. Dufort, M. J. Paszek, V. M. Weaver, *Nat. Rev. Mol. Cell Biol.* **2011**, *12*, 308.

- [4] J. D. Humphrey, E. R. Dufresne, M. A. Schwartz, *Nat. Rev. Mol. Cell Biol.* **2014**, *15*, 802.
- [5] C. Yang, M. W. Tibbitt, L. Basta, K. S. Anseth, *Nat. Mater.* **2014**, *13*, 645.
- [6] K. Uto, J. H. Tsui, C. A. DeForest, D.-H. Kim, *Prog. Polym. Sci.* **2017**, *65*, 53.
- [7] J. Kim, R. C. Hayward, *Trends Biotechnol.* **2012**, *30*, 426.
- [8] E. R. Ruskowitz, C. A. DeForest, *Nat. Rev. Mater.* **2018**, *3*, 17087.
- [9] S. Khetan, J. S. Katz, J. A. Burdick, *Soft Matter* **2009**, *5*, 1601.
- [10] S. Khetan, J. A. Burdick, *Biomaterials* **2010**, *31*, 8228.
- [11] S. Khetan, M. Guvendiren, W. R. Legant, D. M. Cohen, C. S. Chen, J. A. Burdick, *Nat. Mater.* **2013**, *12*, 458.
- [12] M. S. Hahn, J. S. Miller, J. L. West, *Adv. Mater.* **2006**, *18*, 2679.
- [13] K. A. Mosiewicz, L. Kolb, A. J. van der Vlies, M. P. Lutolf, *Biomater. Sci.* **2014**, *2*, 1640.
- [14] J. L. Young, A. J. Engler, *Biomaterials* **2011**, *32*, 1002.
- [15] G. P. Raeber, M. P. Lutolf, J. A. Hubbell, *Biophys. J.* **2005**, *89*, 1374.
- [16] J. Patterson, J. A. Hubbell, *Biomaterials* **2010**, *31*, 7836.
- [17] A. M. Kloxin, A. M. Kasko, C. N. Salinas, K. S. Anseth, *Science* **2009**, *324*, 59.
- [18] C. A. DeForest, K. S. Anseth, *Nat. Chem.* **2011**, *3*, 925.
- [19] P. Martens, T. Holland, K. S. Anseth, *Polymer* **2002**, *43*, 6093.
- [20] C. A. DeForest, K. S. Anseth, *Annu. Rev. Chem. Biomol. Eng.* **2012**, *3*, 421.
- [21] J. A. Burdick, W. L. Murphy, *Nat. Commun.* **2012**, *3*, 1269.
- [22] M. W. Tibbitt, K. S. Anseth, *Sci. Transl. Med.* **2012**, *4*, 160ps24.
- [23] A. M. Rosales, K. S. Anseth, *Nat. Rev. Mater.* **2016**, *1*, 15012.
- [24] J. D. Ehrick, S. K. Deo, T. W. Browning, L. G. Bachas, M. J. Madou, S. Daunert, *Nat. Mater.* **2005**, *4*, 298.
- [25] W. L. Murphy, W. S. Dillmore, J. Modica, M. Mrksich, *Angew. Chem., Int. Ed.* **2007**, *46*, 3066.
- [26] W. Yuan, J. Yang, P. Kopečková, J. Kopeček, *J. Am. Chem. Soc.* **2008**, *130*, 15760.
- [27] B. M. Gillette, J. A. Jensen, M. Wang, J. Tchao, S. K. Sia, *Adv. Mater.* **2010**, *22*, 686.
- [28] S. Tamesue, Y. Takashima, H. Yamaguchi, S. Shinkai, A. Harada, *Angew. Chem., Int. Ed.* **2010**, *49*, 7461.
- [29] D. C. Lin, B. Yurke, N. A. Langrana, *J. Mater. Res.* **2005**, *20*, 1456.
- [30] L. Peng, M. You, Q. Yuan, C. Wu, D. Han, Y. Chen, Z. Zhong, J. Xue, W. Tan, *J. Am. Chem. Soc.* **2012**, *134*, 12302.
- [31] N. Kong, Q. Peng, H. Li, *Adv. Funct. Mater.* **2014**, *24*, 7310.
- [32] W. H. Rombouts, D. W. De Kort, T. T. H. Pham, C. P. M. van Mierlo, M. W. T. Werten, F. A. De Wolf, J. van der Gucht, *Biomacromolecules* **2015**, *16*, 2506.
- [33] X. Zhou, C. Li, Y. Shao, C. Chen, Z. Yang, D. Liu, *Chem. Commun.* **2016**, *52*, 10668.
- [34] A. M. Rosales, K. M. Mabry, E. M. Nehls, K. S. Anseth, *Biomacromolecules* **2015**, *16*, 798.
- [35] X. Wu, W. Huang, W. H. Wu, B. Xue, D. Xiang, Y. Li, M. Qin, F. Sun, W. Wang, W. Bin Zhang, Y. Cao, *Nano Res.* **2017**, *1*, <http://doi.org/10.1007/s12274-017-1890-y>.
- [36] A. M. Rosales, C. B. Rodell, M. H. Chen, M. G. Morrow, K. S. Anseth, J. A. Burdick, *Bioconjugate Chem.* **2018**, *29*, 905.
- [37] H. M. Berman, J. Westbrook, Z. Feng, G. Gilliland, T. N. Bhat, H. Weissig, I. N. Shindyalov, P. E. Bourne, *Nucleic Acids Res.* **2000**, *28*, 235.
- [38] C. A. DeForest, B. D. Polizzotti, K. S. Anseth, *Nat. Mater.* **2009**, *8*, 659.
- [39] C. A. DeForest, E. A. Sims, K. S. Anseth, *Chem. Mater.* **2010**, *22*, 4783.
- [40] C. A. DeForest, K. S. Anseth, *Angew. Chem., Int. Ed.* **2012**, *51*, 1816.
- [41] C. A. DeForest, D. A. Tirrell, *Nat. Mater.* **2015**, *14*, 523.
- [42] B. A. Badeau, M. P. Comerford, C. K. Arakawa, J. A. Shadish, C. A. DeForest, *Nat. Chem.* **2018**, *10*, 251.
- [43] O. Boutoureira, G. J. L. Bernardes, *Chem. Rev.* **2015**, *115*, 2174.
- [44] B. Devadas, T. Lu, A. Katoh, N. S. Kishore, A. C. Wade, P. P. Mehta, D. A. Rudnick, M. L. Bryant, S. P. Adams, Q. Li, G. Gokel, J. I. Gordon, *J. Biol. Chem.* **1992**, *267*, 7224.
- [45] W. P. Heal, M. H. Wright, E. Thinon, E. W. Tate, *Nat. Protoc.* **2012**, *7*, 105.
- [46] C. Kulkarni, T. L. Kinzer-Ursem, D. A. Tirrell, *ChemBioChem* **2013**, *14*, 1958.
- [47] H. Mao, S. A. Hart, A. Schink, B. A. Pollok, *J. Am. Chem. Soc.* **2004**, *126*, 2670.
- [48] C. P. Guimaraes, M. D. Witte, C. S. Theile, G. Bozkurt, L. Kundrat, A. E. M. Blom, H. L. Ploegh, *Nat. Protoc.* **2013**, *8*, 1787.
- [49] K. Wagner, M. J. Kwakkenbos, Y. B. Claassen, K. Majoor, M. Böhne, K. F. van der Sluijs, M. D. Witte, D. J. van Zoelen, L. A. Cornelissen, T. Beaumont, A. Q. Bakker, H. L. Ploegh, H. Spits, *Proc. Natl. Acad. Sci. USA* **2014**, *111*, 16820.
- [50] D. Rabuka, *Curr. Opin. Chem. Biol.* **2010**, *14*, 790.
- [51] A. Miyawaki, J. Llopis, R. Heim, J. M. McCaffery, J. A. Adams, M. Ikura, R. Y. Tsien, *Nature* **1997**, *388*, 882.
- [52] J. Nakai, M. Ohkura, K. Imoto, *Nat. Biotechnol.* **2001**, *19*, 137.
- [53] Y. N. Tallini, M. Ohkura, B.-R. Choi, G. Ji, K. Imoto, R. Doran, J. Lee, P. Plan, J. Wilson, H.-B. Xin, A. Sanbe, J. Gulick, J. Mathai, J. Robbins, G. Salama, J. Nakai, M. I. Kotlikoff, *Proc. Natl. Acad. Sci. USA* **2006**, *103*, 4753.
- [54] Y. Zhao, S. Araki, J. Wu, T. Teramoto, Y.-F. Chang, M. Nakano, A. S. Abdelfattah, M. Fujiwara, T. Ishihara, T. Nagai, R. E. Campbell, *Science* **2011**, *333*, 1888.
- [55] D. Cai, L. Ren, H. Zhao, C. Xu, L. Zhang, Y. Yu, H. Wang, Y. Lan, M. F. Roberts, J. H. Chuang, M. J. Naughton, Z. Ren, T. C. Chiles, *Nat. Nanotechnol.* **2010**, *5*, 597.
- [56] N. J. Greenfield, *Nat. Protoc.* **2007**, *1*, 2876.
- [57] I. S. Carrico, B. L. Carlson, C. R. Bertozzi, *Nat. Chem. Biol.* **2007**, *3*, 321.
- [58] P. J. Flory, J. Rehner, *J. Chem. Phys.* **1943**, *11*, 521.
- [59] D. E. Clapham, *Cell* **2007**, *131*, 1047.
- [60] A. Möglich, K. Moffat, *Photochem. Photobiol. Sci.* **2010**, *9*, 1286.
- [61] L. Fenu, O. Yizhar, K. Deisseroth, *Annu. Rev. Neurosci.* **2011**, *34*, 389.
- [62] E. Pastrana, *Nat. Methods* **2011**, *8*, 24.
- [63] C. Renicke, D. Schuster, S. Usherenko, L.-O. Essen, C. Taxis, *Chem. Biol.* **2013**, *20*, 619.
- [64] J. M. Christie, *Annu. Rev. Plant Biol.* **2007**, *58*, 21.
- [65] S. J. Bryant, C. R. Nuttelman, K. S. Anseth, *J. Biomater. Sci., Polym. Ed.* **2000**, *11*, 439.
- [66] D. Y. Wong, T. Ranganath, A. M. Kasko, *PLoS One* **2015**, *10*, e0139307.
- [67] M. Salomon, J. M. Christie, E. Knieb, U. Lempert, W. R. Briggs, *Biochemistry* **2000**, *39*, 9401.
- [68] B. Hinz, S. H. Phan, V. J. Thannickal, A. Galli, M.-L. Bochaton-Pia llat, G. Gabbiani, *Am. J. Pathol.* **2007**, *170*, 1807.
- [69] O. Kanisicak, H. Khalil, M. J. Ivey, J. Karch, B. D. Maliken, R. N. Correll, M. J. Brody, S.-C. J. Lin, B. J. Aronow, M. D. Tallquist, J. D. Molkenin, *Nat. Commun.* **2016**, *7*, 12260.
- [70] R. G. Wells, *Hepatology* **2008**, *47*, 1394.
- [71] A. Stempien-Otero, D. H. Kim, J. Davis, *J. Mol. Cell. Cardiol.* **2016**, *97*, 153.
- [72] J. Davis, A. R. Burr, G. F. Davis, L. Birnbaumer, J. D. Molkenin, *Dev. Cell* **2012**, *23*, 705.
- [73] J. D. Molkenin, D. Bugg, N. Ghearing, L. E. Dorn, P. Kim, M. A. Sargent, J. Gunaje, K. Otsu, J. Davis, *Circulation* **2017**, *136*, 549.
- [74] J. Davis, N. Salomonis, N. Ghearing, S.-C. J. Lin, J. Q. Kwong, A. Mohan, M. S. Swanson, J. D. Molkenin, *Nat. Commun.* **2015**, *6*, 10084.
- [75] H. A. Van Valkenburgh, R. A. Kahn, *Methods Enzymol.* **2002**, *344*, 186.
- [76] R. Warden-Rothman, I. Caturegli, V. Popik, A. Tsourkas, *Anal. Chem.* **2013**, *85*, 11090.